

Journal Name

Crossmark

PAPER

RECEIVED
dd Month yyyy

REVISED
dd Month yyyy

[Minimizing energy dissipation during programming of resistive switching memory devices using their dynamical attractor states]

Valeriy A. Slipko¹, Alon Ascoli², Fernando Corinto² and Yuriy V. Pershin^{3,*}

¹Institute of Physics, Opole University, Opole 45-052, Poland

²Department of Electronics and Telecommunications Politecnico di Torino, Turin, Italy

³Department of Physics and Astronomy, University of South Carolina, Columbia, SC 29208 USA

*Author to whom any correspondence should be addressed.

E-mail: vslipko@uni.opole.pl, alon.ascoli@polito.it, fernando.corinto@polito.it, and pershin@physics.sc.edu

Keywords: ReRAM devices, memristive devices, resistance switching memory, optimal control, energy minimization

Abstract

Under certain conditions, applying a sequence of voltage pulses of alternating polarities across a resistive switching memory device induces a finite number of fixed-point attractors, known as dynamical attractors. Remarkably, dynamical attractors can be used to program analog values into the device state without supervision. Because different pulse sequences can produce the same trajectory solution for the state in the phase space, there is strong potential for optimization, particularly in regard to the energy cost of the programming phase, which this study addresses. Without loss of generality, the proposed theory-based energy minimization strategy is applied to the voltage threshold adaptive memristor model, known for its predictive capability and adaptability to fit a large number of resistance switching memory devices. The optimization design crafts ad-hoc pulse sequences, that minimize the energy required to program the device into a desired dynamical attractor state. The theoretical approach is also extended to cover situations, where a fast programming scheme should be adopted to serve time-critical electronics applications.

1 Introduction

The precise programming of resistance switching memory devices [1] is crucial for various applications that depend on memristive states. These applications include analog circuits using memristive devices [2], memristive neural networks [3, 4, 5], and crossbar-based memory arrays that can also function as computing engines, such as accelerating matrix-vector multiplications [6, 7, 8]. On one hand, the effectiveness of memristive technologies heavily relies on the precision during the state programming process. On the other hand, developing methods to reduce power dissipation in a memristive device during programming is critically important, especially in mobile technical systems with limited energy supplies.

In general, applying a sequence of voltage pulses of alternating polarity across a resistance switching memory device can induce a finite number of dynamical attractors in the device's phase space, opening up novel and intriguing opportunities for device programming. This concept was introduced in [9] and further explored in [10], [11], [12], [13], and [14]. Moreover, in [15], high-frequency periodic signals were used to induce controlled resistance switching transitions in non-volatile memristor devices endowed with fading memory [16]. Importantly, in recent years, several studies explored the theoretical basis behind the synthesis of low-power programming schemes for memristive devices [17, 18, 19]. One notable finding is that the stimulus, minimizing Joule losses in ideal memristors, corresponds to constant power dissipation [17].

This study merges the areas of dynamical attractors and low-power programming of memristive devices. Specifically, we present a theoretical framework that designs a programming pulse sequence to minimize Joule losses within the device while simultaneously producing a desired dynamic attractor. Our analysis is based on the voltage threshold adaptive memristor (VTEAM)

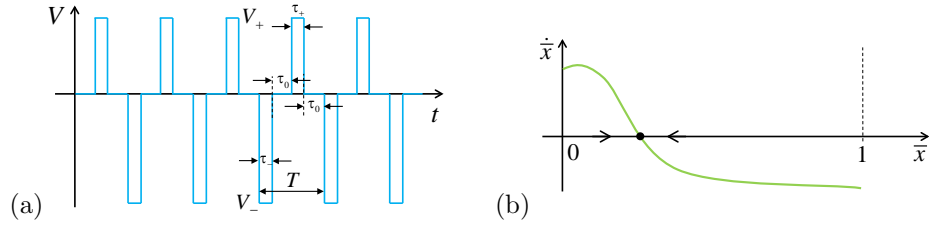


Figure 1. Illustration of the dynamical attractor concept for a first-order memristive device. (a) Pulse sequence, consisting, over each cycle, of a pair of pulses of alternating amplitudes V_+ and V_- and corresponding widths τ_+ and τ_- , and let fall across the memristive device during the programming phase. T is the pulse train period, τ_0 the inter-pulse interval. (b) Schematic plot demonstrating the time-averaged flow of a time-averaged internal state variable, referred to as \bar{x} , for the device under the periodic pulse train excitation sketched in (a). The arrow pointing to the right (left) indicates a progressive increase (decrease) in the time-averaged state from cycle to cycle. The dot marks the position of an attractor, which the pulse train stimulus induces in the phase space of the memristive device. Adapted from [10].

model [20] that is a particular realization of first-order memristive devices and systems [21]

$$I(t) = G_M(x, V) V(t), \quad (1)$$

$$\dot{x} = f(x, V). \quad (2)$$

Here, I and V are the current through and the voltage across the device, respectively, $G_M(x, V)$ stands for the *memory conductance*, memductance for short, x represents some internal state variable, and $f(x, V)$ denotes the *state evolution function*. As demonstrated experimentally [22], physical resistive switching memory devices are not (ideal) memristors and therefore their response can be described by the first-order (Eqs. (1)-(2)) or higher-order memristive model [21], rather than the memristor model [23].

Figure 1 schematically represents the concept of dynamical attractors [9]. A necessary requirement for the presence of a dynamical attractor, for a device periodically stimulated by a pulse sequence, is the dependence of the state evolution function $f(x, V)$ in Eq. (2) on x [9]. In first-order memristive systems, the point $x = x_a$ is a fixed-point attractor if Eqs. (3) and (5) in Ref. [9] are simultaneously satisfied. An essential characteristic of a fixed-point attractor is the convergence of trajectories towards the attractor from its basin of attraction. During this process, the system loses information about its initial state, demonstrating fading memory [16]. Importantly, dynamical attractors are not limited to devices described by first-order models [9].

This paper is organized as follows. In Sec. 2, we present the VTEAM model and derive a time-averaged trajectory solution for the internal state of a resistance switching memory device, under pulse train excitation. Sec. 3.1 outlines the objectives of the state programming operation, while the remainder of Sec. 3 describes the proposed theoretical methodology for synthesizing the most energy-efficient state programming protocol (Sec. 3.2) and the most energetically-favorable programming scheme under a limited time budget (Sec. 3.3). Joule losses across memristive devices under programming are assessed in Sec. 4. The discussion of our results can be found in Sec. 5. The paper concludes with a conclusion.

2 Model and trajectory

2.1 VTEAM model

Our study is based on the VTEAM model [20]. In this model, Eq. (2) has the following form:

$$\frac{dx}{dt} = f(x, V) = \begin{cases} k_{off} \left(\frac{V}{v_{off}} - 1 \right)^{\alpha_{off}} f_{off}(x), & 0 < v_{off} < V, \\ 0, & v_{on} < V < v_{off}, \end{cases} \quad (3)$$

$$\frac{dx}{dt} = f(x, V) = \begin{cases} k_{on} \left(\frac{V}{v_{on}} - 1 \right)^{\alpha_{on}} f_{on}(x), & V < v_{on} < 0, \end{cases} \quad (4)$$

$$k_{off} > 0, k_{on} < 0, \alpha_{off} > 0, \alpha_{on} > 0 \quad (5)$$

where $k_{off} > 0$, $k_{on} < 0$, $\alpha_{off} > 0$, $\alpha_{on} > 0$ are constant parameters, whereas $f_{off}(x)$ and $f_{on}(x)$ are window functions, restricting the allowable variation range of the state variable x , denoting the normalized width of the insulating part of the functional layer within the device physical stack, to the closed interval $[x_{on}, x_{off}]$, with $x_{on} = 0$ and $x_{off} = 1$, and reading as

$$f_{off}(x) = 1 - x,$$

and

$$f_{on}(x) = x,$$

respectively. According to the state evolution function $f(x, V)$ (Eqs. (3)-(5)), the device undergoes RESET/SET resistance switching transitions when the applied to the device voltage V is above/below a positive/negative threshold level v_{off}/v_{on} .

The memductance $G_M(x, V)$, which appears in the generalized Ohm's law (1), is selected as

$$G_M(x) = G_{max} + (G_{min} - G_{max})x, \quad (6)$$

where G_{min} and G_{max} are the minimum and maximum conductance levels, corresponding to $x_{off} = 1$ and $x_{on} = 0$, respectively.

2.2 Trajectory

In the limit of narrow pulses, the time-averaged dynamics of pulse-driven memristors can be described by the equation [11]

$$\dot{\bar{x}}(t) = \frac{1}{T} (f(\bar{x}, V_+) \tau_+ + f(\bar{x}, V_-) \tau_-), \quad (7)$$

where T is the pulse sequence period, V_{\pm} are the pulse amplitudes, and τ_{\pm} are the pulse durations, see Fig. 1. Defining

$$A = k_{off} \left(\frac{V_+}{v_{off}} - 1 \right)^{\alpha_{off}} \frac{\tau_+}{T} \quad (8)$$

and

$$B = k_{on} \left(\frac{V_-}{v_{on}} - 1 \right)^{\alpha_{on}} \frac{\tau_-}{T}, \quad (9)$$

Eq. (7) is rewritten as

$$\dot{\bar{x}}(t) = A(1 - \bar{x}) + B\bar{x}. \quad (10)$$

The solution of Eq. (10) is given by

$$\bar{x}(t) = \frac{A}{A - B} + \left(x_0 - \frac{A}{A - B} \right) e^{-(A - B)t}, \quad (11)$$

where $x(t = 0) = x_0$ denotes the initial condition (state). In Eq. (11), the first term represents the location of a stable fixed point, which we denote by

$$x_a \equiv \frac{A}{A - B}, \quad (12)$$

while the second term describes the relaxation process from the initial state x_0 towards the equilibrium point x_a . The corresponding relaxation time is defined via $\tau_r \equiv (A - B)^{-1}$. Note that the memristor state trajectory $x(t)$ is fully and uniquely defined by the constants A and B , and by the initial condition x_0 . Here we emphasize that $B < 0$, as it follows from Eqs. (9) and from the negative sign of k_{on} (see the line directly following Eq. (5)).

In principle, the Joule losses across the device are defined by the exact trajectory $x(t)$ of the state variable and time-dependent voltage. However, in the limit of narrow pulses, the exact trajectory $x(t)$ may be well approximated by the time-averaged trajectory $\bar{x}(t)$. Under these circumstances the Joule losses can be estimated accurately via

$$Q[x(t), V(t)] \approx \frac{1}{T} (V_+^2 \tau_+ + V_-^2 \tau_-) \int_0^{t_f} G_M(\bar{x}(t)) dt, \quad (13)$$

where t_f denotes the programming time. Eq. (13) forms the basis for the optimization strategy proposed in this work.

3 Optimal trajectory design

3.1 Objectives of state programming

As programming objectives, we select the following two parameters: the location of the stable fixed point, x_a , and the point-to-point amplitude ϵ of long-time oscillations of $x(t)$ about x_a . The latter parameter establishes the accuracy of the state programming. In the following, we demonstrate that the parameters A and B in Eqs. (8) and (9) are determined by these two programming objectives. For the reader's ease, Fig. 3(c) below displays the meaning of the parameters x_a and ϵ .

Now, consider the amplitude of oscillations of $x(t)$ about x_a in the long-time limit. Accounting for Eq. (2), which describes the full dynamics, the changes in the internal state due to positive and negative pulses can be approximately expressed as [10] $\Delta_+ = f(x_a, V_+) \tau_+$ and $\Delta_- = f(x_a, V_-) \tau_-$, such that $\Delta_+ + \Delta_- = 0$. The parameter ϵ is introduced as $\epsilon \equiv |\Delta_{\pm}|$. For the VTEAM model, taking into account Eqs. (3), (5), (8) and (9), one finds

$$AT(1 - x_a) = \epsilon, \quad (14)$$

$$-BTx_a = \epsilon. \quad (15)$$

Consequently, the parameters A and B can be expressed as

$$A = \frac{\epsilon}{T(1 - x_a)}, \quad (16)$$

$$B = -\frac{\epsilon}{Tx_a}. \quad (17)$$

Once the values of A and B are set, Eqs. (8) and (9) provide relationships between the amplitudes and durations of negative and positive pulses. In particular, the durations can be expressed as

$$\tau_+(V_+) = \frac{\epsilon}{k_{off} \left(\frac{V_+}{v_{off}} - 1 \right)^{\alpha_{off}} (1 - x_a)}, \quad (18)$$

$$\tau_-(V_-) = -\frac{\epsilon}{k_{on} \left(\frac{V_-}{v_{on}} - 1 \right)^{\alpha_{on}} x_a}. \quad (19)$$

Eqs. (18) and (19) demonstrate that to attain greater precision (i.e., smaller ϵ -s), one must employ shorter pulses.

3.2 The most energy efficient programming scheme

This subsection assumes that the pulse period T , another parameter in Eqs. (16) and (17), is long enough to implement the most energy-efficient sequences. The opposite case is considered in Sec. 3.3 below.

With A and B determined (refer to Eqs. (16) and (17)), the pre-integral factor in Eq. (13) remains the sole element available for minimization. Our energy loss minimization procedure applies separately to pulses of positive and negative polarity. By substituting τ_+ from Eq. (18) into Eq. (13), for the positive pulse, the optimization problem reduces to

$$\hat{V}_+ = \underset{v_{off} \leq V_+ \leq V_+^{max}}{\operatorname{Argmin}} \frac{V_+^2}{\left(\frac{V_+}{v_{off}} - 1 \right)^{\alpha_{off}}}, \quad (20)$$

where V_+^{max} is the most positive voltage to which the device may be subjected, and the hat symbol denotes the *optimal* pulse amplitude. The minimization of Joule losses under RESET switching transitions results in the requirement to choose the height of the negative pulses according to

$$\hat{V}_- = \underset{V_-^{max} \leq V_- \leq v_{on}}{\operatorname{Argmin}} \frac{V_-^2}{\left(\frac{V_-}{v_{on}} - 1 \right)^{\alpha_{on}}}, \quad (21)$$

where V_-^{max} is the most negative voltage applicable across the device.

Eq. (20) leads to

$$\hat{V}_+ = \begin{cases} \min \left\{ \frac{2}{2 - \alpha_{off}} v_{off}, V_+^{max} \right\}, & \text{for } \alpha_{off} < 2, \\ V_+^{max}, & \text{for } \alpha_{off} \geq 2. \end{cases} \quad (22)$$

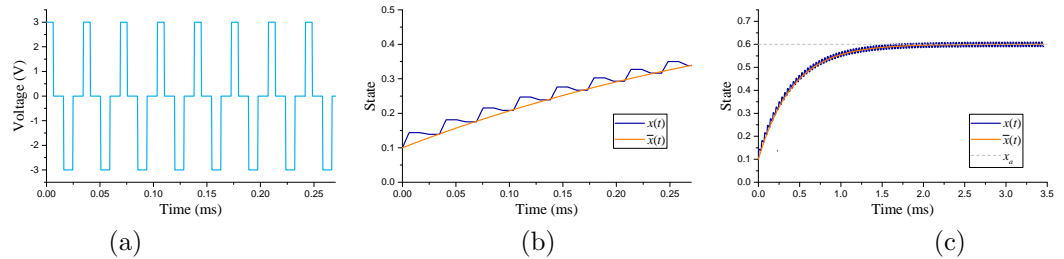


Figure 2. Example of optimal control based upon the following parameter setting: $v_{off/on} = \pm 1$ V, $\alpha_{off} = 3$, $\alpha_{on} = 2$, $k_{off/on} = \pm 10^3$, $V_{\pm}^{max} = \pm 3$ V, $x_0 = 0.1$, $x_a = 0.6$, $\epsilon = 0.02$, $\tau_0 = 10$ μ s. Here, plot (a) shows the control voltage pulse sequence, where $\hat{V}_+ = V_+^{max} = 3$ V and $\hat{V}_- = V_-^{max} = -3$ V according to Eqs. (22) and (23), respectively, while $\tau_+ = 6.3$ μ s and $\tau_- = 8.3$ μ s as follows in turn from Eqs. (18) and (19). The pulse sequence admitted then an input period T of 34.6 μ s, as computed via Eq. (24). Plots (b) and (c) depict the memristor state response to the pulse train in (a) over the initial phase and across the entire programming time, respectively. In (b) and (c), the smooth line represents the analytical solution according to Eq. (11).

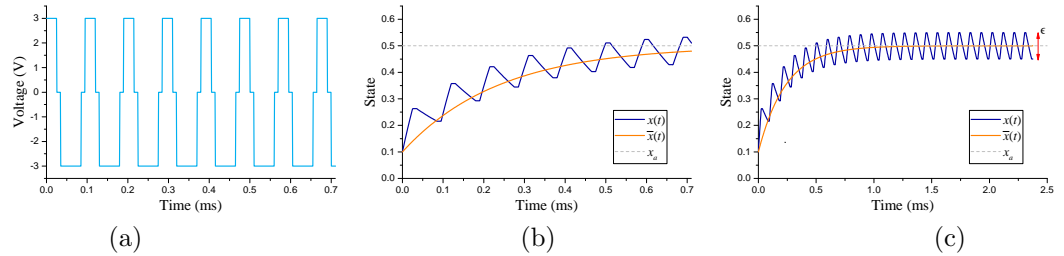


Figure 3. Example of optimal control based upon the same parameter setting as in Fig. 2, except for x_a , and ϵ , here taken equal to 0.5 and 0.1, respectively. See the caption of Fig. 2 for the significance of the curves in plots (a), (b), and (c). For this simulation, according to Eqs. (22) and (23) \hat{V}_+ and \hat{V}_- were respectively set to $V_+^{max} = 3$ V and $V_-^{max} = -3$ V, as in Fig. 2. As a result, using the formulas (18) and (19), τ_+ and τ_- were in turn chosen equal to 25 μ s and 50 μ s. From equation (24), the pulse sequence period T was thus found to amount to 95 μ s.

Similarly,

$$\hat{V}_- = \begin{cases} \max \left\{ \frac{2}{2 - \alpha_{on}} v_{on}, V_-^{max} \right\}, & \text{for } \alpha_{on} < 2, \\ V_-^{max}, & \text{for } \alpha_{on} \geq 2. \end{cases} \quad (23)$$

Eqs. (18) and (19) enable the determination of pulse widths for given pulse amplitudes (refer to Eqs. (22) and (23)). The pulse period T can be found as follows:

$$T_{opt} = \tau_+(\hat{V}_+) + \tau_-(\hat{V}_-) + 2\tau_0, \quad (24)$$

where $2\tau_0$ is the total duration of the time interval across which $V = 0$ within the pulse period. Our findings are applicable to both symmetric (as shown in Fig. 1, bottom) and asymmetric arrangements of alternating pulses within a period; what truly matters is solely the total length of the zero-input time interval, namely, $2\tau_0$. Note that $\tau_+(\hat{V}_+) + \tau_-(\hat{V}_-)$ is the shortest period of the optimal pulse sequence.

Figs. 2-4 illustrate examples of optimal sequences obtained through the method outlined in the current subsection.

3.3 The most energetically-favourable yet fast programming scheme

In some cases, it may be necessary to restrict the programming time, even if this leads to Joule losses that are higher than the minimal level obtainable with the sequences outlined earlier in subsection 3.2.

In all possible scenarios, the shortest pulse period is

$$T_{min} = \tau_+(V_+^{max}) + \tau_-(V_-^{max}) \leq T_{opt} \quad (25)$$

as the highest pulse amplitude corresponds to the shortest pulse duration (see Eqs. (18) and (19)). An interesting case is when the desired pulse sequence period T satisfies

$$T_{min} < T < T_{opt}|_{\tau_0=0}. \quad (26)$$

In fact, there are two related cases:

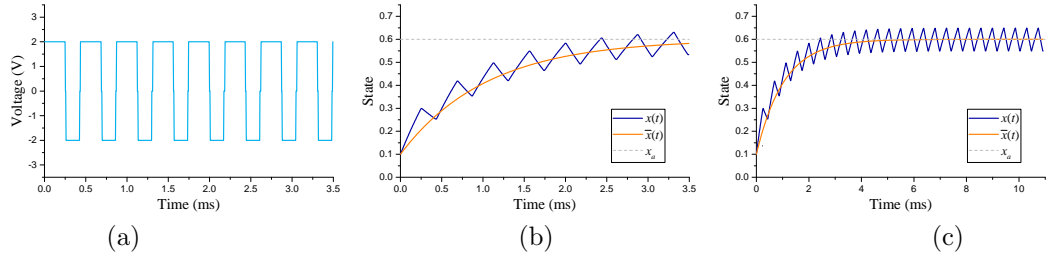


Figure 4. Example of optimal control based upon the same parameter setting as in Fig. 2, except for $\alpha_{off/on}$, and ϵ , here set equal to 1 and 0.1, respectively. Here the inequalities $V_+^{max} > 2v_{off}/(2 - \alpha_{off})$ and $|V_-^{max}| < 2v_{on}/(2 - \alpha_{on})$ hold true. Refer to the caption of Fig. 2 for information on the traces in plots (a), (b), and (c). For this simulation Eqs. (22) and (23) respectively set the optimal RESET and SET pulse amplitudes, i.e., in turn, \hat{V}_+ and \hat{V}_- , to $2v_{off}/(2 - \alpha_{off}) = 2V$ and $2v_{on}/(2 - \alpha_{on}) = -2V$, respectively. As a result, τ_+ and τ_- were set to 250 μ s and 167 μ s, on the basis of Eqs. (18) and (19), respectively. Therefore, T was found to be equal to 437 μ s according to equation (24).

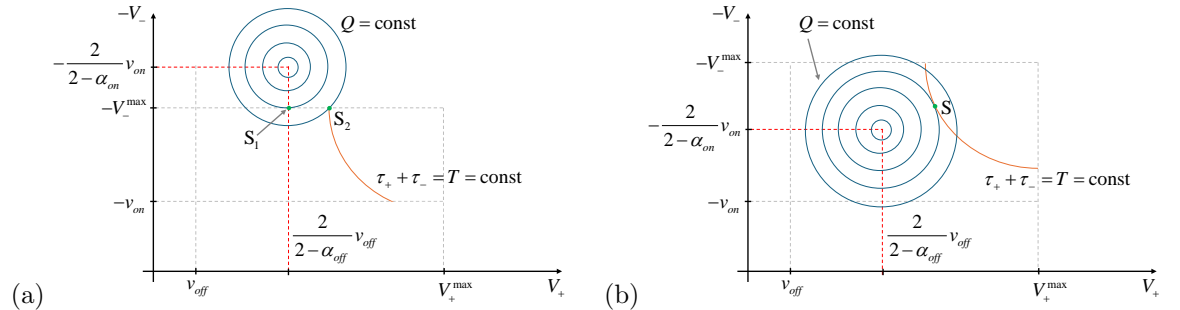


Figure 5. Minimizing Joule losses in the presence of constraints on pulse amplitudes and widths in the case where $\alpha_{off} < 2$ and $\alpha_{on} < 2$. The allowable variation ranges for V_+ and for $-V_-$ are (v_{off}, V_+^{max}) and $(-v_{on}, -V_-^{max})$, respectively. (a) A schematic illustration of the scenario where $V_+^{max} > 2v_{off}/(2 - \alpha_{off})$ and $|V_-^{max}| < 2|v_{on}|/(2 - \alpha_{on})$. (b) A schematic illustration of the scenario where $V_+^{max} > 2v_{off}/(2 - \alpha_{off})$ and $|V_-^{max}| > 2|v_{on}|/(2 - \alpha_{on})$. It is worth observing that, when both inequalities $\alpha_{on} < 2$ and $\alpha_{off} < 2$ apply, the contours of the function $Q = Q(V_+, V_-)$ are closed loci, which originates from the fact that in situations of this kind there always exists finite positive and negative pulse amplitudes, in turn V_+ and V_- , at which Joule losses are minimized under RESET and SET transitions, respectively, in the unconstrained case (refer to Fig. 6(b)). On the other hand, in case α_{on} and/or α_{off} were larger than or equal to 2, the contours of the function $Q = Q(V_+, V_-)$ would be open curves. In scenarios of this kind, if the first (second) inequality from the aforementioned pair held true, the most energetically-favourable SET (RESET) pulse amplitudes V_- (V_+) would be negative (positive) infinity under unconstrained conditions (refer to Fig. 6(a)). Refer to the text for additional information.

3.3.1 Case 1 Consider the scenario, where Eqs. (22) and (23) suggest selecting the pulse amplitude pair $\{\hat{V}_+ = V_+^{max}, \hat{V}_- = 2v_{on}/(2 - \alpha_{on})\}$. This scenario occurs if a) $\alpha_{off} \geq 2$ or $\alpha_{off} < 2$ and $V_+^{max} < 2v_{off}/(2 - \alpha_{off})$ and b) $\alpha_{on} < 2$ and $|V_-^{max}| > 2|v_{on}|/(2 - \alpha_{on})$. Let us however also assume that for the application of interest, employing the optimal pulse sequence to program the device would exceed the maximum allowable time. This would call for the adoption of a faster programming protocol, so that the pulse train period T could satisfy the constraint Eq. (26). In this case, the amplitude for the positive pulse is selected as \hat{V}_+ , τ_+ is computed via (18), and, concurrently, the width of the negative pulse is calculated as the remainder of the pulse sequence period, i.e via

$$\tau_- = T - \tau_+(\hat{V}_+). \quad (27)$$

Then, the amplitude of the negative pulse can be found by solving Eq. (19) for V_- , while using τ_- from Eq. (27).

Let us now consider the scenario, where Eqs. (22) and (23) result in the optimal pulse amplitude pair choice $\{\hat{V}_+ = 2v_{off}/(2 - \alpha_{off}), \hat{V}_- = V_-^{max}\}$. This scenario occurs if a) $\alpha_{on} \geq 2$ or $\alpha_{on} < 2$ and $|V_-^{max}| < 2|v_{on}|/(2 - \alpha_{on})$ and b) $\alpha_{off} < 2$ and $V_+^{max} > 2v_{off}/(2 - \alpha_{off})$. Now, let us suppose the memristor-centered application requires the implementation of a fast resistance switching scheme, as dictated by the constraint (26), so as to prevent the programming time to exceed a predefined upper bound. In a situation of this kind, the amplitude for the negative pulse is selected as \hat{V}_- , τ_- is computed via (19), and, concurrently, the width of the positive pulse is calculated as the remainder of the pulse sequence period, i.e via

$$\tau_+ = T - \tau_-(\hat{V}_-). \quad (28)$$

Then, the amplitude of the positive pulse can be found by solving Eq. (18) for V_+ , while using τ_+ from Eq. (28). In fact, a schematic diagram of this case is presented in Fig. 5(a) when $\alpha_{on} < 2$ and $\alpha_{off} < 2$. Here, the coordinates of the point “S₁” represent the optimal pulse amplitudes when $\tau_+ + \tau_- = T_{opt}|_{\tau_0=0}$. However, under the constraint, defined through Eq. (26), the most energetically-favorable solution turns out to be inferable from the coordinates of the point “S₂”, where a constant-value contour of the function $Q(V_+, V_-) = \text{const}$ crosses the curve associated with the condition

$$\tau_+ + \tau_- = T \quad (29)$$

along the line $V_- = V_-^{max}$. The resulting pulse sequence would induce a larger energy dissipation across the device than the optimal one presented in Sec. (3.2). This is the price to pay to program the device resistance at a higher rate.

3.3.2 Case 2 Another possibility emerges when Eqs. (22) and (23) suggest setting the amplitudes of the pulse sequence as $\{\hat{V}_+ = 2v_{off}/(2 - \alpha_{off}), \hat{V}_- = 2v_{on}/(2 - \alpha_{on})\}$, which is the case when the inequalities $\alpha_{on} < 2$ and $\alpha_{off} < 2$ hold true, while, concurrently, $V_+^{max} > 2v_{off}/(2 - \alpha_{off})$ and $|V_-^{max}| > 2|v_{on}|/(2 - \alpha_{on})$. Yet the period T_{opt} of the most energetically-favourable pulse train would be too long to keep the duration of the programming phase below a given application-dependent upper bound. The optimization task would then involve the minimization of Q , as given in Eq. (13), under the condition (29), which may be achieved by recurring to the standard method of the Lagrange multipliers [24].

Fig. 5(b) illustrates the method graphically. The most energetically-favourable solution in the fast programming scheme corresponds to the point “S”, where a contour of the function $Q(V_+, -V_-)$ is tangent to the curve illustrating the constraint expressed by Eq. (29)). Mathematically, this condition boils down to

$$\nabla Q(V_+, V_-) = \lambda \nabla (\tau_+ + \tau_-), \quad (30)$$

where ∇ represents the gradient operator, and λ is the Lagrange multiplier. Eq. (30) may be expanded as

$$\frac{\frac{\partial Q(V_+, V_-)}{\partial V_+}}{\frac{\partial \tau_+(V_+)}{\partial V_+}} = \frac{\frac{\partial Q(V_+, V_-)}{\partial V_-}}{\frac{\partial \tau_-(V_-)}{\partial V_-}}. \quad (31)$$

The location of the point “S” in Fig. 5(b) can be found by solving simultaneously Eqs. (29) and (31) for V_+ and V_- . The widths τ_+ and τ_- of the positive and negative pulse are then computed by means of Eqs. (18) and (19), respectively.

4 Joule losses

Having established the optimal programming protocols in Sec. 3, we are now in a perfect position for evaluating the Joule losses in the memristive device during the programming phase. Our starting point is Eq. (13). The integral in Eq. (13) can be calculated analytically, leading to the closed-form expression

$$I \equiv \int_0^{t_f} G_M(\bar{x}(t)) dt = G_M(x_a)t_f + (x_0 - x_a)(G_{min} - G_{max}) \left(1 - e^{-\frac{t_f}{\tau_r}} \right) \tau_r. \quad (32)$$

On the right-hand side of Eq. (32), the first term is proportional to the programming time t_f and accounts for Joule losses associated with the attractor state. Meanwhile, the second term is a finite contribution related to the transient relaxation dynamics occurring over the time scale τ_r . This contribution may be either positive or negative, depending on the location of x_0 with respect to x_a .

Within Eq. (13), the programming time t_f is yet to be determined. Taking into account the exponential behavior given by Eq. (11), the relaxation time $\tau_r = (A - B)^{-1}$ emerges as a suitable time scale to define t_f . Practically, one should allow for a time span of several relaxation times to ensure the device to attain a location adequately close to the attractor. As a result, we suggest choosing t_f according to the specification

$$t_f = p\tau_r, \quad (33)$$

where p is a real number generally falling within the range [2, 5] in most applications.

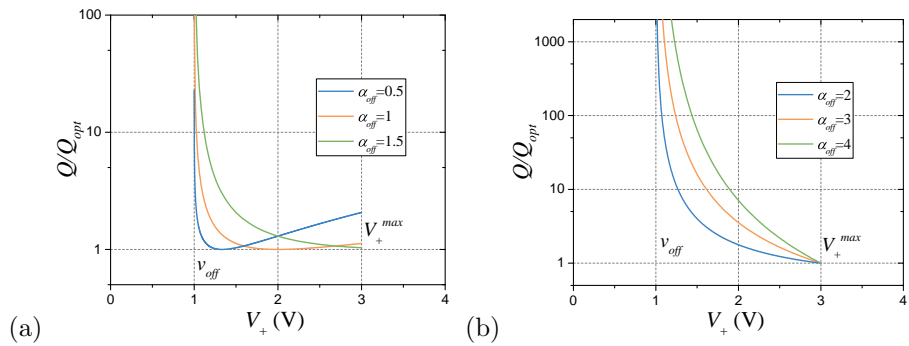


Figure 6. Device energy dissipation Q relative to its optimal counterpart Q_{opt} under positive pulse excitation for $v_{off} = 1$ V and $V_+^{max} = 3$ V, when (a) $\alpha_{off} < 2$ and (b) $\alpha_{off} \geq 2$. The calculations were performed for a device with symmetric kinetics (assuming $\alpha_{on} = \alpha_{off}$, $v_{on} = -v_{off}$, $V_-^{max} = -V_+^{max}$), and the same trajectory $\bar{x}(t)$.

Here we point out that Eq. (32) remains invariate across various program protocols (assuming the same trajectory). Variations arise from the pre-integral coefficient in Eq. (13), which must be addressed individually for different pulsing scenarios. In all cases, however, the Joule losses in the memristive device may be accurately evaluated inspecting the closed-form expression

$$Q = \left[\frac{\epsilon V_+^2}{k_{off} \left(\frac{V_+}{v_{off}} - 1 \right)^{\alpha_{off}} (1 - x_a)} - \frac{\epsilon V_-^2}{k_{on} \left(\frac{V_-}{v_{on}} - 1 \right)^{\alpha_{on}} x_a} \right] \frac{I}{T}, \quad (34)$$

where I is given by Eq. (32). Below are a few examples for illustration.

To illustrate the strategy outlined in Sect. 3.2, Fig. 6 displays the programming energy Q versus the pulse amplitude V_+ , relative to the optimal value Q_{opt} . This figure was generated for a device with symmetric kinetics, considering each value of the parameters α_{off} of the set $\{0.5, 1, 1.5\}$ in panel (a) and from the set $\{2, 3, 4\}$ in panel (b). In the present case, Q/Q_{opt} remains constant regardless of the details of the trajectory, since the I/T factor in Eq. (34) is the same for the same trajectory.

For the simulation scenario illustrated in Fig. 4, Fig. 7 presents a comparison between the Joule losses in the device, as calculated on the basis of the time-averaged trajectory $\bar{x}(t)$, utilizing our theoretical formula (34), and on the precise trajectory $x(t)$, employing equations (3)-(5), respectively.

5 Discussion

Although many experiments on memristive devices have focused on the precision of state programming, another fundamental aspect, namely its energy efficiency, has attracted far less experimental attention [25]. In this study, we have introduced a method to optimize energy cost for programming a non-volatile resistance switching memory device using its dynamical attractor state [9]. This state is reached through the application of a specific sequence of alternating pulses from any initial state, thus in the presence of a fading memory effect, as described in [16]. It has been found that a particular pulses sequence that minimizes the energy cost depends on several model parameters.

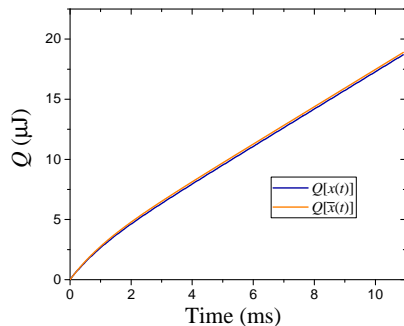


Figure 7. Comparison between the Joule losses, expected to occur through the device in the programming scenario from Fig. 4, as determined from the exact trajectory $x(t)$, acquired from the numerical integration of the VTEAM model, and from the respective time-averaged solution $\bar{x}(t)$ on the basis of the proposed formula (34). Here G_{min} and G_{max} were respectively taken equal to 10^{-5} S and to 10^{-3} S.

5.1 Programming sequence

Figure 2 illustrates an example in which the exponents α_{off} and α_{on} in the state evolution function $f(x, V)$ (see Eqs. (3) and (5)) are greater than or equal to 2. In this context, which assumes the VTEAM model is tailored to a device with asymmetric SET and RESET switching kinetics, the optimal strategy involves using pulses with the maximum potential amplitude ($|\hat{V}_\pm| = 3$ V).

Conversely, Fig. 4 details a different case where the VTEAM model is adapted for a device with symmetric SET and RESET switching kinetics. Here, both α_{off} and α_{on} are less than 2, and the conditions $V_+^{max} > 2v_{off}/(2 - \alpha_{off})$ and $|V_-^{max}| > 2|v_{on}|/(2 - \alpha_{on})$ are satisfied. From Eq. (22) ((23)), it follows that an intermediate positive (negative) voltage level, specifically $\hat{V}_+ = 2v_{off}/(2 - \alpha_{off}) = 2$ V ($\hat{V}_- = 2v_{on}/(2 - \alpha_{on}) = -2$ V), should be used for the RESET and SET pulse heights, respectively, to achieve the most energy-efficient programming operation when applying the periodic voltage pulse train across the device.

Figure 3 was generated using the same model parameters as Fig. 2, except for ϵ and x_a , which are larger and smaller, respectively, than in the simulation that produced Fig. 2. By comparing Figs. 2 and 3, it can be observed that increasing ϵ from 0.02 to 0.1 results in more pronounced oscillations in the state variable $x(t)$.

5.2 Joule losses

Figure 6 illustrates the Joule losses predicted by our theoretical model as a function of the amplitude of the RESET pulse. In Fig. 6(a), a scenario is presented where $\alpha_{off} < 2$, suggesting a parameter-based RESET pulse configuration for optimal energy efficiency. In this case, the curve Q/Q_{opt} versus V_+ has a minimum at $V_+ = 2v_{off}/(2 - \alpha)$ for any value α . However, the minimum's abscissa of this curve falls within (or outside) the range (v_{off}, V_+^{max}) for $\alpha_{off} \in (0, 4/3)$ ($\alpha_{off} \in (4/3, 2)$). In the latter situation, \hat{V}_+ should be set to the upper limit V_+^{max} within the permissible range.

In contrast, Fig. 6(b) presents the scenario where $\alpha_{off} \geq 2$, showing that the lowest energy cost is obtained when the maximum positive pulse is used. Here, regardless of the specific value assigned to α_{off} , the energy Q dissipated in the device, compared to its optimal counterpart Q_{opt} , consistently reduces to 1 when $V_+ = V_+^{max}$.

The theoretical development of curves like those shown in Fig. 6 can result in substantial energy savings during the critical and essential task of programming resistances in memristive devices.

Conclusion

In conclusion, dynamical attractor states of memristive devices offer an alternative approach to their programming. This research has investigated methods to reduce energy consumption within this framework. Using the VTEAM model, we have evaluated our theory-based optimization strategy to show how energy dissipation in the device can be minimized when exposed to voltage pulses of alternating polarity.

The optimal pulse sequence depends on the critical parameters α_{off} and α_{on} , which play a key role in the device's switching kinetics. When the former (latter) parameter is 2 or higher, the optimal energy-efficient strategy is to select the highest possible magnitude for RESET (SET) pulses. On the other hand, if α_{off} (α_{on}) is less than 2, achieving maximum energy efficiency requires setting the RESET (SET) pulse magnitude to the lesser of a certain intermediate voltage magnitude and highest possible voltage magnitude (taking into account the polarity).

Our theory-driven optimization strategy demonstrates that choosing optimized pulse sequences can significantly decrease energy dissipation in memristive devices during repeated programming operations. This theoretical method has also been utilized to explore the reduction of energy dissipation in memristive devices under fast programming schemes, which could be beneficial for real-time edge computing applications. Our theoretical approach is set to be compared with experimental data from real-world implementations of memristive devices in the future.

Acknowledgement

YVP was supported by the NSF grant EFRI-2318139.

References

- [1] Ielmini D and Waser R 2016 *Resistive Switching: From Fundamentals of Nanoionic Redox Processes to Memristive Device Applications* (Wiley-VCH)
- [2] Pershin Y V and Di Ventra M 2010 *IEEE Trans. Circuits Syst. I* **57** 1857–1864

- [3] Pershin Y V and Di Ventra M 2010 *Neural networks* **23** 881–886
- [4] Kang S M, Choi D, Eshraghian J K, Zhou P, Kim J, Kong B S, Zhu X, Demirkol A S, Ascoli A, Tetzlaff R, Lu W D and Chua L O 2021 *IEEE Trans. Circuits Syst. I* **68** 4837–4850
- [5] Ascoli A, Tetzlaff R, Kang S and Chua L 2020 *IEEE Trans. Circuits Syst. I* **67** 2753 – 2766
- [6] Hu M, Graves C E, Li C, Li Y, Ge N, Montgomery E, Davila N, Jiang H, Williams R S, Yang J J, Xia Q and Strachan J P 2018 *Advanced Materials* **30** 1705914
- [7] Woods W and Teuscher C 2017 Approximate vector matrix multiplication implementations for neuromorphic applications using memristive crossbars *2017 IEEE/ACM International Symposium on Nanoscale Architectures (NANOARCH)* pp 103–108
- [8] Amirsoleimani A, Alibart F, Yon V, Xu J, Pazhouhandeh M R, Ecoffey S, Beilliard Y, Genov R and Drouin D 2020 *Advanced Intelligent Systems* **2** 2000115
- [9] Pershin Y V and Slipko V A 2019 *Europhysics Letters* **125** 20002
- [10] Pershin Y V and Slipko V A 2019 *Journal of Physics D: Applied Physics* **52** 505304
- [11] Slipko V A and Pershin Y V 2019 *Physica E: Low-dimensional Systems and Nanostructures* **114** 113561
- [12] Ascoli A, Schmitt N, Messaris I, Demirkol A, Tetzlaff R and Chua L 2023 *Frontiers in Electronic Materials* **23** (32pp.)
- [13] Ascoli A, Schmitt N, Messaris I, Demirkol A, Strachan J, Tetzlaff R and Chua L 2024 *Scientific Reports* **14** (29pp.)
- [14] Schmitt N, Ascoli A, Messaris I, Demirkol A, Menzel S, Rana V, Tetzlaff R and Chua L O 2024 *Frontiers in Nanotechnology* **6** 1301320
- [15] Messaris I, Demirkol A, Ascoli A and Tetzlaff R 2023 *IEEE Trans. Circuits Syst. I* **70** 566–578
- [16] Ascoli A, Tetzlaff R, Chua L, Strachan J and Williams R 2016 *IEEE Trans. Circuits Syst. I* **63** 389–400
- [17] Slipko V A and Pershin Y V 2025 *IEEE Transactions on Nanotechnology* **24** 8–16
- [18] Astin N and Pershin Y V 2025 *arXiv preprint arXiv:2507.18487*
- [19] Slipko V A, Ascoli A, Corinto F and Pershin Y V 2025 *arXiv preprint arXiv:2508.15620*
- [20] Kvatinsky S, Ramadan M, Friedman E G and Kolodny A 2015 *IEEE Trans. Circuits Syst. II* **62** 786–790
- [21] Chua L O and Kang S M 1976 *Proceedings of IEEE* **64** 209–223
- [22] Kim J, Pershin Y V, Yin M, Datta T and Di Ventra M 2020 *Advanced Electronic Materials* **6** 2000010
- [23] Chua L O 1971 *IEEE Transactions on Circuit Theory* **18** 507–519
- [24] Arfken G B, Weber H J and Harris F E 2011 *Mathematical methods for physicists: A comprehensive guide* (Academic press)
- [25] Fleck K, Böttger U, Waser R, Aslam N, Hoffmann-Eifert S and Menzel S 2016 Energy dissipation during pulsed switching of strontium-titanate based resistive switching memory devices *2016 46th European Solid-State Device Research Conference (ESSDERC)* (IEEE) pp 160–163